Estimating human trabecular meshwork stiffness by numerical modeling and advanced OCT imaging

Ke Wang[1], Murray A. Johnstone[2], Chen Xin[3], Shaozhen Song[3], Steven Padilla[2], Janice A. Vranka[4], Ted S. Acott[4], Kai Zhou[1], Stephen A. Schwaner[1], Ruikang K. Wang[3], Todd Sulchek[5], C. Ross Ethier[1, 5*]

[1] Department of Biomedical Engineering, Georgia Institute of Technology/Emory University, Atlanta, GA

[2] Department of Ophthalmology, University of Washington, Seattle, WA

[3] Department of Bioengineering, University of Washington, Seattle, WA

[4] Department of Ophthalmology, Casey Eye Institute, Portland, Oregon

[5] George W. Woodruff School of Mechanical Engineering, Georgia Institute of Technology, Atlanta, GA

1. Supplemental Material

Methods

Mesh refinement study

For 2D modelling approach, it is important to ensure that any finite element mesh is sufficiently refined so that the numerical simulations based on that mesh are not prone to significant numerical error, while also minimizing required computing time. To test this, we carried out a mesh refinement study on the finite element model created from quadrant 77R-IN. All parameters including boundary conditions, loading pressure, and tissue stiffness remained the same. TM stiffness was set at 114 kPa. Simulations were run for a series of different element sizes which were characterized by edge length.

3D model

With the pseudo-2D modelling approach, the model geometry was created based only on tissue structures observed from a single 2D OCT slice. The tissue regions modeled in 2D at a single location were unable to adequately characterize the TLS oriented circumferentially in SC and therefore, it was impossible to depict those tissue structures which spanned several slices. Thus, a 3D model, including tissue structures such as TLS, collector channel and septae, was built and the estimated TM stiffnesses were compared between the 2D and 3D approaches.

Specifically, a 3D model was built for the superior temporal quadrant of eye 80R to compare against the 2D approach. The geometry for the 3D model was based on 9 adjacent OCT images, instead of a single image as for the pseudo-2D models. The central OCT image used in the 3D model was the same as that in pseudo-2D model for eye 80R, giving a 3D model thickness of 80 μm thus allowing us to include potentially relevant outflow tissue structures such as transluminal structures (TLS), septa and a collector channel (CC) (Figure S1). Cornea/Sclera

and CB were given the same stiffness values as those in pseudo-2D model. In the absence of any specific data, septae were assigned a stiffness which was close to that of TM. A pressure load was applied to all inner surfaces of the open SC and CC lumens, with a magnitude identical to that applied in the pseudo-2D model of the same quadrant. This did not precisely replicate the experimental situation, but allowed a direct comparison between results of the pseudo-2D model and the 3D model. As with the pseudo-2D models, the SC lumen configuration was compared between simulated and experimentally measured results. Specifically, the difference in SC area at the higher pressure (in this case 30 mmHg) of the 3D model was computed as

$$\Delta\text{Area} = \sqrt{\sum_{n=1}^{9}(Area_{OCT\_layer\_n} - Area_{FEM\_layer\_n})^2} \quad \text{(S1)}$$

where the index n refers to summation over the OCT cross-sections that the model was constructed from. This quantity was computed for different TM stiffnesses. The best match between computed and experimentally measured SC area was achieved at a TM stiffness of 48 kPa, which can be compared to 60 kPa obtained from the pseudo-2D model.

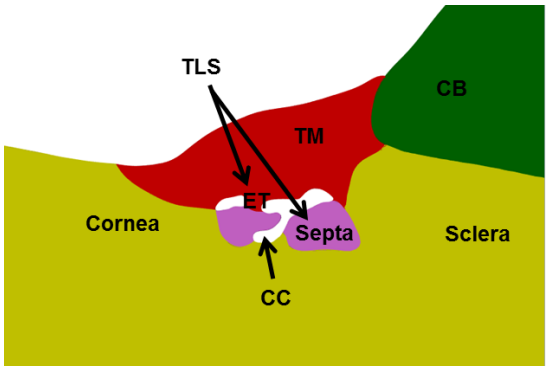

Figure S1: One cross-section of the 3D model for superior quadrant of eye 80R. TM = trabecular meshwork, CB = ciliary body, TLS = Trans Luminal Structure, ET = Endothelial lining, CC = collector channel.

Sensitivity analysis

In practice, the biomechanical properties of outflow tissue other than the TM can vary from sample to sample. In addition, manual tissue boundary delineation may differ from reality and is somewhat subjective. We thus performed a sensitivity analysis on these aspects of the simulations in the 2D modelling approach.

First, the effects of sclera/cornea and ciliary body stiffnesses on predicted TM stiffness were evaluated using Latin Hypercube Sampling (LHS). LHS is an efficient stratified sampling technique where each input variable in a simulation is described by a probability distribution which is decomposed into equi-probable intervals [1]. For each simulation, a value for each variable is randomly selected from one equi-probable interval, without replacement. These input variables are used to drive a numerical simulation, and this process is repeated for many combinations of input variable values. An advantage of LHS is that it efficiently provides sensitivity information, which in this case was used to determine how changes in two variables (sclera/cornea stiffness and CB stiffness) impacted on estimated TM stiffness. The minimum number of required simulations, N, for a LHS study has been empirically established as $N > 4k/3$, where k is the number of input variables [1, 2]. In this study, fifteen random combinations of sclera/cornea and CB stiffnesses were generated by LHS, which satisfied the above criterion.

A key step in the LHS process is specifying the probability distributions of the input variables. We took mean stiffnesses for sclera/cornea and CB to be 3000 kPa and 100 kPa, respectively, as in the preliminary simulations. The stiffness range for normal human sclera/cornea was taken as 1000 – 5000 kPa [3, 4]. CB stiffness varied from 30 – 170 kPa. The lower and upper bounds for the CB stiffness were assumed to be mean ± 0.7*mean, to match the proportional range for sclera/cornea. Values in both ranges were assumed to be uniformly distributed.

Next, the effect of boundary delineation on estimated TM stiffness was tested using three different TM/CB delineations, where the boundary between the two tissue structures was most ambiguous and indistinguishable as observed in OCT images (Figure 2). Three different plausible CB delineations were established (Figure S2) and the analysis was repeated for each delineation.

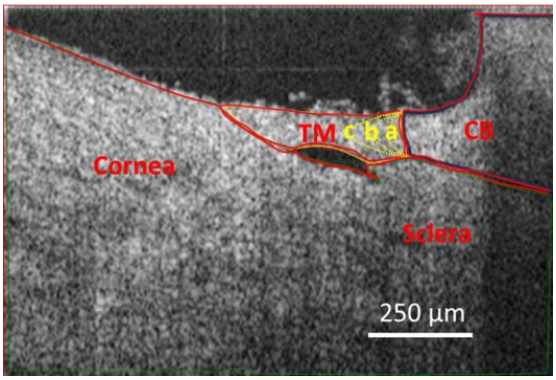

Figure S2: Different TM/CB boundary delineations. Three possible TM/CB boundaries (a - c) are indicated by yellow dashed lines overlain on an OCT image. Sample: inferior nasal quadrant of Eye 77R.

Corrected loading pressure

Finally, we realized that the pressure within the SC lumen is not necessarily the same as the reservoir pressure because of flow resistance in the system. For FE modeling, we must apply a pressure load that is consistent with the real situation in order to accurately simulate tissue deformation. The following shows how we estimated the relevant flow resistances and thus luminal SC pressures, using quadrant 77R-IN as an example.

Resistance Calculation in the OCT-based Inflation Test System:

(1) *Resistance of tubing:* There were 6 sections of tubing with known inner diameters (ID) and lengths (Figure S3) in the system. We assumed the tubing to be cylindrical and thus used Poiseuille flow (Equation S2) to calculate the hydrodynamic flow resistance to flow

$$R_{cylinder} = \frac{128\mu L}{\pi D^4} \quad \text{(S2)}$$

where μ is the viscosity of saline, taken as 1 cP; L is the length of the tubing; and D is the inner diameter of the tubing.

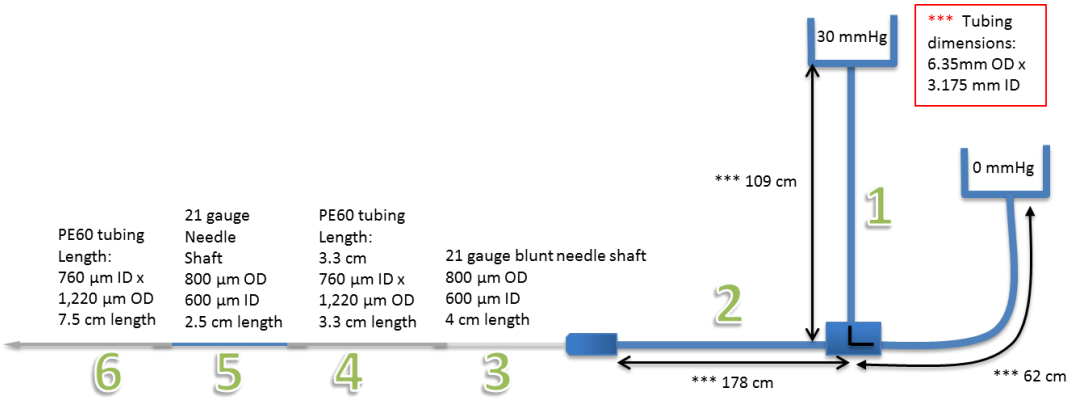

Figure S3: Schematic diagram of tubing system upstream of cannula. All tubing segments are numbered and labeled with inner and outer diameters.

(2) *Resistance of cannula:* The dimensions of the cannula were measured on several 3D OCT images using Fiji software and are shown in Figure S4. The cross-sections of the cannula were taken to be ellipses. Since both semi-major and semi-minor axes of the ellipses are functions of the distance from cannula tip, the resistance of cannula could be calculated by treating the flow as locally Poiseuille and integrating along the length of the cannula [18], as follows:

$$R_{cannula} = \int_0^L \frac{4\mu\left(b^2(x)+c^2(x)\right)}{\pi b^3(x)c^3(x)}\,dx \quad \text{(S3)}$$

where $b(L)$ and $c(L)$ are the local semi-major and –minor axes of the ellipse; μ is the viscosity of saline; L is the length of the cannula and $R_{cannula}$is the cannula resistance.

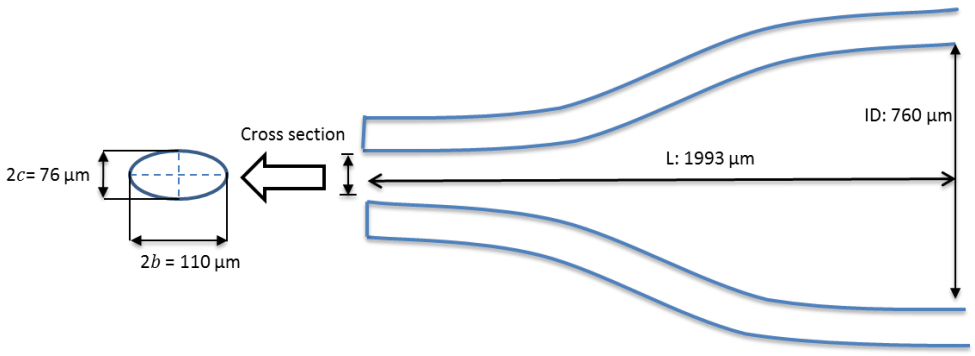

Figure S4: Schematic view of the cannula. b: semi-major axis of ellipse; c: semi-minor axis of ellipse

(3) *Resistance of SC:* We assume the SC lumen to be a cylinder with elliptic cross section. The SC lumen resistance (R_{SC}) can be calculated as follows:

$$R_{SC} = \frac{4\mu L_{SC}(b_{SC}^2+c_{SC}^2)}{\pi b_{SC}^3 b_{SC}^3} \quad \text{(S4)}$$

where b_{SC} and c_{SC} are the semi-major and –minor axes of the elliptic SC cross section measured by ImageJ (Version 1.5, National Institutes of Health, Bethesda MD) from OCT scans; μ is the viscosity of saline; and L_{SC} is the length of SC. L_{SC} was approximated as 8 mm since each quadrant is one fourth of the anterior eye, which made it about 9 mm, and one millimeter was taken off for wastage from cutting and trimming, etc.

The distance from the tip of the cannula to the scan location was about 2 mm. Thus, the pressure at the scan location (P_{scan}) was equal to the pressure drop from scan location to the free end of the SC, which had a length of three fourths of the total SC length for this specific quadrant:

$$P_{scan} = \frac{3}{4} R_{SC} \times Q \quad \text{(S5)}$$

where Q is the flow rate along the SC (see equation S6). We assumed the pressure on the free end of SC (Figure S5) was zero referenced to the bath pressure.

$$Q = \frac{P_{reservoir}}{R_{tubing}+R_{cannula}+R_{SC}} \quad \text{(S6)}$$

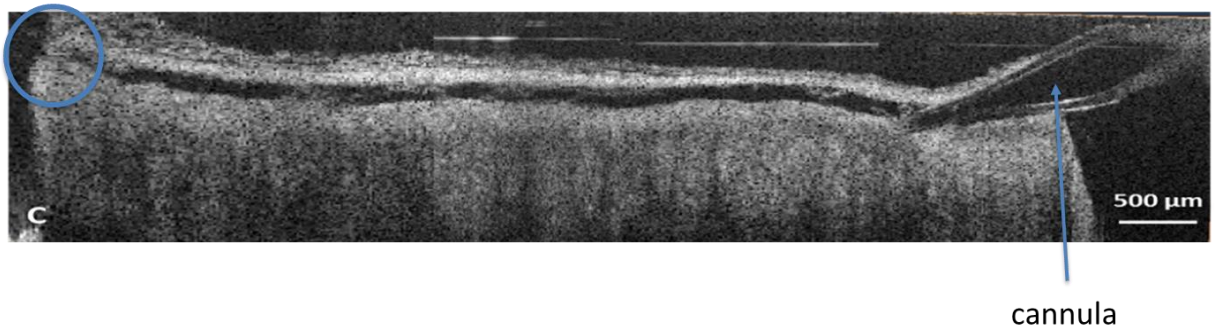

Figure S5: Representative cross-sectional OCT image containing the entire SC lumen. Cannula was inserted into the right side of the SC. The region inside the blue circle shows apparent *SC* collapse, which was occasionally seen in some samples.

Results

Mesh refinement study

The predicted SC perimeter and area both converged to asymptotic values as the mesh element size was reduced (Figure S6). Based on these results, an edge length of c. 7 μm was judged suitable to balance accuracy and computational cost, which was approximately the average element size we used for our models (5 – 10 μm).

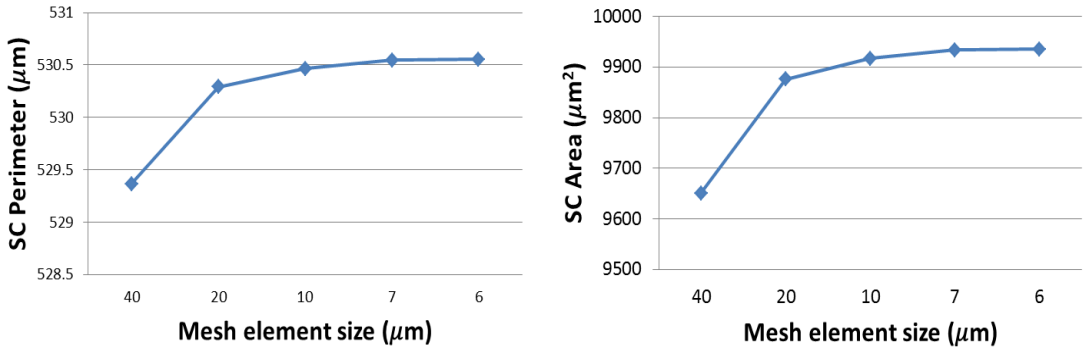

Figure S6: Mesh refinement test for FEM simulation. Y axes: SC lumen perimeter (μm) and area (μm^2). X axis: average edge length of hexahedral element (μm). Note inverted scale for x-axis. Sample: inferior nasal quadrant of Eye 77R

3D model

The best match between computed and experimentally measured SC area was achieved at a TM stiffness of 48 kPa (Figure S7), which can be compared to the value of 60 kPa obtained from the pseudo-2D model.

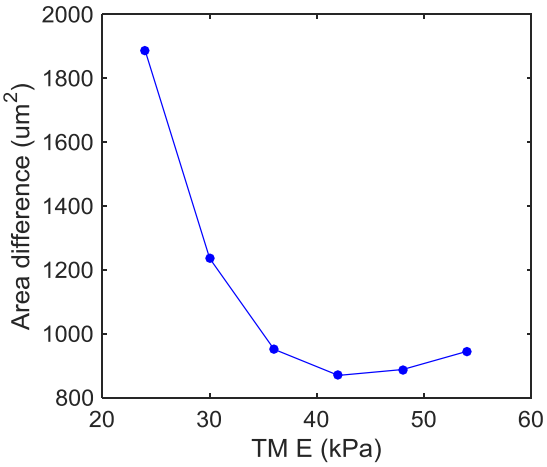

Figure S7: Quantification of SC lumen area difference at a reservoir pressure of 30 mmHg in the 3D model. The X-axis is Young's modulus of TM. Blue curve is the difference between observed and computed SC lumen area. The minimum difference was observed at 48 kPa. Sample: superior temple quadrant of Eye 80R.

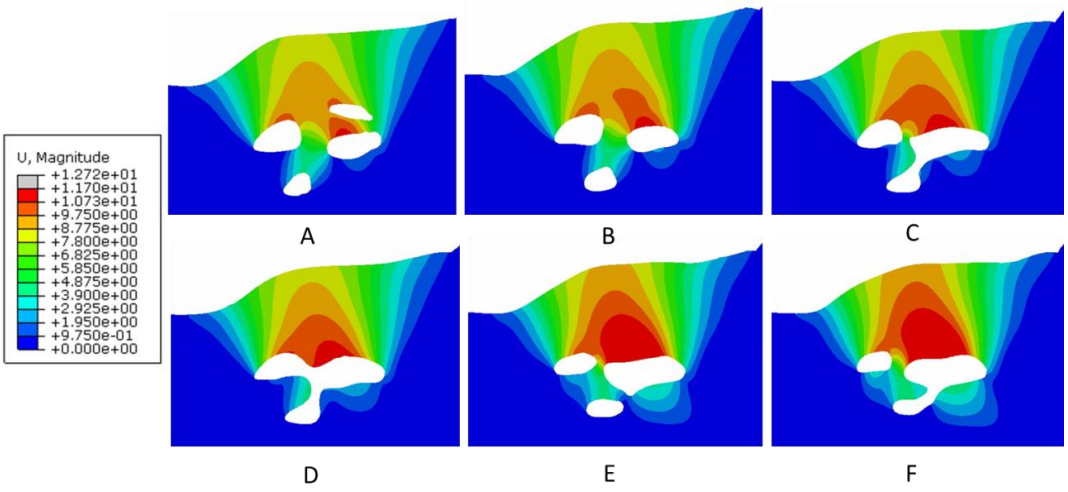

Figure S8: Distribution of the total displacement of the 3D model at 6 different locations (A-F) along the SC lumen. Reservoir pressure = 30 mmHg. Unit of color bar is µm. Sample: superior temple quadrant of Eye 80R.

In addition, our 3D model predicted that, in general, the largest TM displacement occurred in the area around the inner wall of SC and center of the TM (Figure S8). Interestingly, relatively large deformations also appeared in the TLS region which divided the canal into compartments at the entrance of CC (Figure S7, A-C, E-F).

When comparing deformation patterns between the pseudo-2D and 3D models at the same scanning location, the deformation of the outflow tissues looked very similar (Figure S9), except that there was more deformation experienced in the septa region in the 3D model. The slightly lower TM stiffness predicted by the 3D model (48 kPa vs. 60 kPa) might be partially explained by these TLS, since the deformation of those structures suggested that they are in tension and therefore resisted SC lumen distention.

The 3D model had several advantages over the pseudo-2D model. It provided a more realistic tissue geometry which included multiple OCT slices. However, it suffered from some limitations. For example, the exact boundaries of TLS were not entirely clear and the stiffness used for TLS was somewhat arbitrary. In view of the very significant time commitment needed to create such 3D models, and the relatively small difference in predicted TM stiffness between the 3D and pseudo-2D models, we chose to simply use pseudo-2D models in this work.

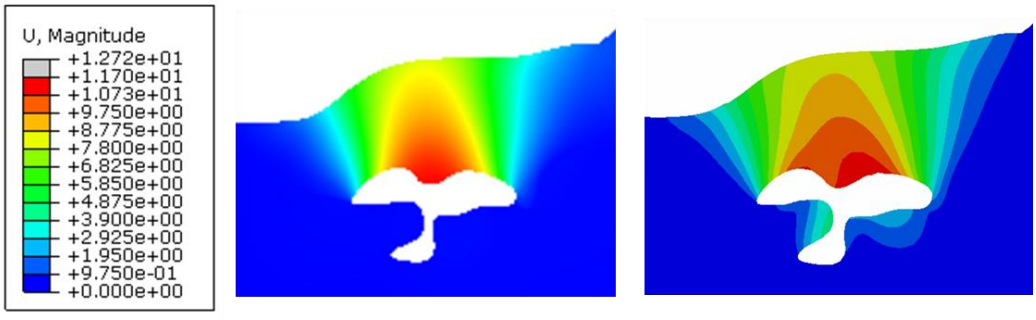

Figure S9: Color map of the total displacement at the same location in 2D (left) and 3D (right) model. Sample: superior temple quadrant of Eye 80R.

Sensitivity analysis

We found that estimated TM stiffnesses were relatively insensitive to variations in input parameters (mean±SD: 122 ± 8.7 kPa for the quadrant considered). In fact, the estimated TM stiffness were between 114-120 kPa for more than 65% of the LHS combinations (Figure S10). Even though statistical analysis suggested that there was a significant partial correlation between two factors (stiffness of sclera/cornea and CB) and the estimated TM stiffness ($p < 0.05$), the squared partial rank correlation coefficients, which is a nonparametric measure of statistical dependence between the ranking of two variables, showed moderate correlations (< 0.5) between CB stiffness and estimated TM stiffness (Table S1). Overall, this analysis indicated that the estimated TM stiffness was insensitive to variation of CB stiffness, which we judged as the major source of material property uncertainty in our simulations.

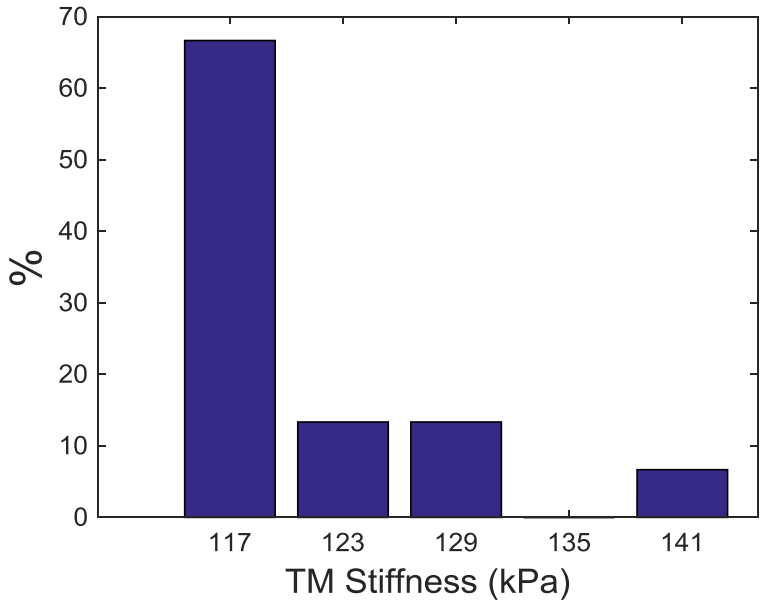

Figure S10: Histogram of estimated TM stiffnesses arising from LHS analysis.

Table S1: Partial correlation between stiffness of two tissue components (sclera/cornea and CB) and TM*

	Sclera/Cornea	CB
prcc^2	0.89	0.45
p-value	< 0.05	< 0.05

*$prcc^2$: squared partial rank correlation coefficient (or Spearman rank correlation coefficient), computed as $prcc = 1 - 6\sum_{i=1}^{N}\frac{D_i}{N(N^2-1)}$, where $D_i$is the difference between the ranks assigned to the corresponding pairs and N is the sample size. Ties are assigned average ranks [5, 6].

For the sensitivity analysis on TM/CB boundary delineation, the estimated TM stiffness (120 kPa) was identical for all three delineations.

In summary, the sensitivity analyses indicated that estimates of TM stiffness were relatively insensitive to both surrounding tissue stiffnesses and boundary delineation between the CB and TM.

Corrected loading pressure

For quadrant 77R-IN, the total tubing resistance (R_{tubing}) and cannula resistance were estimated to be 0.26 and 1.53 mmHg/(μL·s) (Table S2). The resistance of SC was 107.42 mmHg/(μL·s).

Table S2: Resistance of tubing segments

Tubing segment number	Resistance (mmHg/μL·s)
1	0.0033
2	0.0054
3	0.0943
4	0.0302
5	0.0598
6	0.0687

P_{scan} values at different $P_{reservoir}$ values are summarized in Table S3. The difference between P_{scan} and $P_{reservoir}$ is greater when $P_{reservoir}$ is higher.

Table S3: Flow rate and pressure in the experimental system*

	$\boldsymbol{P_{reservoir}}$ **= 5 mmHg (undeformed)**	$\boldsymbol{P_{reservoir}}$ **= 20 mmHg (deformed)**
$\boldsymbol{Q}$	0.05	0.18
$\boldsymbol{P_{scan}}$	3.69	14.75

*Q: flow rate, unit: μL/s; P: pressure, unit: mmHg

2. References

1. Mckay, M.D., R.J. Beckman, and W.J. Conover, *A Comparison of Three Methods for Selecting Values of Input Variables in the Analysis of Output from a Computer Code.* Technometrics, 1979. **21**(2): p. 239-245.
2. Blower, S.M. and H. Dowlatabadi, *Sensitivity and Uncertainty Analysis of Complex-Models of Disease Transmission - an Hiv Model, as an Example.* International Statistical Review, 1994. **62**(2): p. 229-243.
3. McKee, C.T., et al., *Indentation versus tensile measurements of Young's modulus for soft biological tissues.* Tissue Eng Part B Rev, 2011. **17**(3): p. 155-64.
4. Tehrani, S., *Gender difference in the pathophysiology and treatment of glaucoma.* Curr Eye Res, 2015. **40**(2): p. 191-200.
5. Conover, W.J., *Practical Nonparametric Statistics*. Third ed. 1999.
6. al., S.T.P.e., *OMNITAB 80: An Interpretive System for Statistical and Numerical Data Analysis*. 1986: NBS Special Publication 701.